



The effects of die counter-impact on aluminum alloy sheet during electromagnetic forming

Yangzhe Lin¹ · Wei Liu^{1,2} · Zhenghua Meng³ · Xiaoyong Zeng¹ · Shangyu Huang^{1,2}

Received: 23 March 2021 / Accepted: 11 July 2021 / Published online: 21 July 2021

© The Author(s), under exclusive licence to Springer-Verlag London Ltd., part of Springer Nature 2021

Abstract

Electromagnetic forming is a high-speed forming process, and it can generate high contact force between the sheet metal and die. Therefore, the effects of die counter-impact on aluminum alloy sheet during electromagnetic forming were numerically and experimentally investigated. Firstly, the numerical simulations of electromagnetic free forming and electromagnetic die forming were performed with the Gurson-Tvergaard-Needleman damage model. When the aluminum alloy sheet impacted the die, an unignorable normal stress occurred along the thickness direction. The void volume fraction was reduced due to the negative stress triaxiality, and the residual stress became smaller. Secondly, the effect of die counter-impact on the pre-deformed aluminum alloy sheet was numerically inspected for quasi-static and dynamic hybrid electromagnetic forming. Compared with the electromagnetic die forming of aluminum alloy sheet without pre-deformation, the void volume fraction and residual stress reductions were more significant for the pre-deformed aluminum alloy sheet. Finally, the aluminum alloy sheets after different electromagnetic forming experiments were compared by optical microscope and Vickers hardness. The results show that the damage suppression and hardness enhancement are attributed to the effect of die counter-impact, especially for the hybrid quasi-static and dynamic forming processes.

Keywords Electromagnetic forming · Aluminum alloy sheet · Damage · Hardness

1 Introduction

With the requirements of energy saving and emission reduction, lightweight components have become very important in the automobile industry. Aluminum alloy has the advantages of low density, high specific strength, good corrosion resistance, etc. [1]. In the sheet metal forming processes, the damage accumulation will not only lead to crack failure, but also have significant influence on the mechanical properties of

parts in service [2]. However, the damage can be reduced by applying the normal compressive stress to improve the fatigue strength of sheet metal components in some specific forming processes [3].

Electromagnetic forming (EMF) is a high-speed forming technology, which applies the Lorentz force to deform tubular or sheet metal workpiece. It can improve the forming limits and reduce the springback of aluminum alloy sheet [4], but the capability is usually limited to forming small and medium scale parts [5]. For this reason, the hybrid quasi-static and dynamic forming [6] or the electromagnetic-assisted stamping (EMAS) processes [7] were suggested for large-scale and complex parts. Furthermore, the high contact pressure would occur on the sheet metal when it impacts the die at very high speed in EMF, so it is necessary to investigate the effects of die counter-impact on aluminum alloy sheet during EMF and the hybrid quasi-static and dynamic forming processes.

Imbert et al. [8] reported that the forming limit of AA5754 aluminum alloy in electromagnetic die forming was significantly higher than that in electromagnetic free forming, and the main reason was that the interaction between the sheet metal and the die suppresses the damage caused by the

✉ Wei Liu
weiliu@whut.edu.cn

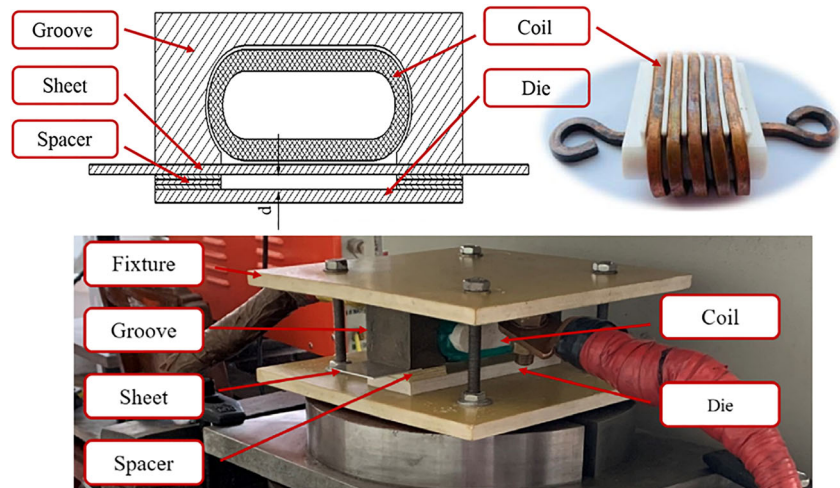
✉ Zhenghua Meng
meng@whut.edu.cn

¹ School of Materials Science and Engineering, Wuhan University of Technology, Wuhan 430070, China

² Hubei Engineering Research Center for Green Precision Material Forming, Wuhan University of Technology, Wuhan 430070, China

³ School of Automotive Engineering, Wuhan University of Technology, Wuhan 430070, China

Fig. 1 Experimental device



forming. Similarly, Golovashchenko et al. [9] found that the formability during V-shaped die forming was significantly improved, while the failure strain during free bulging did not increase. It was mainly attributed to the high-speed collision between the sheet metal and the die. Iriondo et al. [10] performed the electromagnetic shape calibration of U-shaped parts, and found that the impact between the sheet metal and the die can inhibit the springback. By comparing the electromagnetic bending process of the V-shaped parts with the traditional bending process, Kim et al. [11] found that the formability improvement of sheet metal is mainly due to the damage inhibition by the impact between the sheet and the die. Su et al. [12] showed that high-speed impact can be used to optimize the stress distribution, thereby reducing the springback of the workpiece caused by uneven stress distribution. Liu et al. [13] presented the electromagnetic calibration of aluminum alloy surface part after conventional stamping. The mechanism of springback reduction was explained by the plastic deformation improvement and residual stress reduction. Feng et al. [14] discussed the effect of electromagnetic high-speed impact on the performance of sheet metal. They attributed the performance improvement of sheet metal to the significant reduction in grain size and the cross-slip of dislocations. Zeng et al. [15] experimentally and numerically investigated the deformation behavior of

aluminum alloy sheet during electromagnetic forming with uniform pressure coil. The influences of discharge voltage, impact distance, and pre-deformation level on damage evolution were studied. Feng et al. [16] found that in the process of electromagnetic high-speed impact, the change of the surface strain and stress state of the sheet metal by the impact was the main reason for the improvement of the sheet metal forming performance. However, little literature can be found to study the effects of die counter-impact on aluminum alloy sheet during the hybrid quasi-static and dynamic forming or EMAS processes.

In the next sections, the uniform pressure actuator (UPA) was used to obtain homogeneous deformation of AA5754 aluminum alloy sheet for EMF experiments [17]. The GTN damage model was adopted for numerical simulation to predict the damage evolution. The electromagnetic free forming and electromagnetic die forming processes were compared to investigate the effects of die counter-impact on aluminum alloy sheet. Considering the hybrid quasi-static and dynamic forming processes, the aluminum alloy sheet was pre-deformed with the quasi-static tensile strain of 5% and subsequently used for the electromagnetic free forming and electromagnetic die forming experiments. The results

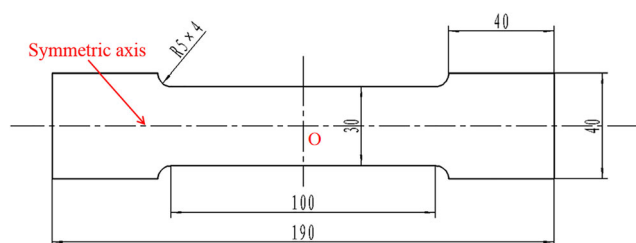


Fig. 2 Geometry of specimen (unit, in millimeters)

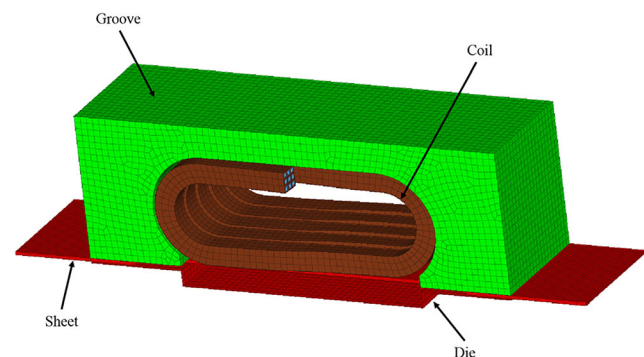


Fig. 3 The numerical model

Table 1 The electromagnetic parameters [13]

Category	Parameters	Value
RLC circuit	Resistance (mΩ)	15
	Inductance (μH)	3
	Capacitance (μF)	550
	Groove (MS m ⁻¹)	36
Electrical conductivity	Sheet (MS m ⁻¹)	36
	Coil (MS m ⁻¹)	58

can provide some understanding for the EMF process design to set properties of aluminum alloy sheet parts.

2 Experimental and simulation methods

2.1 Experimental procedures

The EMF experiments were performed with the WG-II EMF machine developed by Wuhan University of Technology. The maximum discharge energy of the EMF machine is about 60 kJ, the maximum storage capacity is 660 μF, and the maximum discharge voltage is 11 kV. The experimental device was mainly composed of the coil, groove, die, spacer, and fixtures, as shown in Fig. 1. The UPA was used as the electromagnetic coil in the experiment to obtain homogeneous deformation. The cross-section of coil was 6 mm × 6 mm, the number of turns was 5, and the turn spacing was 2 mm. This coil was made of copper due to the high electrical conductivity, and it was wound on a polyester model. The epoxy resin and curing agent were mixed and injected between the groove and the coil. The groove was pressed by the fixtures to well contact with aluminum alloy sheet for the electrical current loop. The distance d between the workpiece and the die was changed by the number or thickness of spacer, so the impact condition was modified with the constant discharge parameters.

Table 2 The parameters of GTN model [8]

Parameters	Value
Initial void volume fraction f_0	0.0
Initial void nucleating particle fraction f_N	0.03
Average nucleation strain ε_N	0.05
Standard deviation of nucleation strain S_N	0.01
Coalescence void volume fraction f_c	0.03
Failure void volume fraction f_F	0.2
q_1	1.5
q_2	1.0

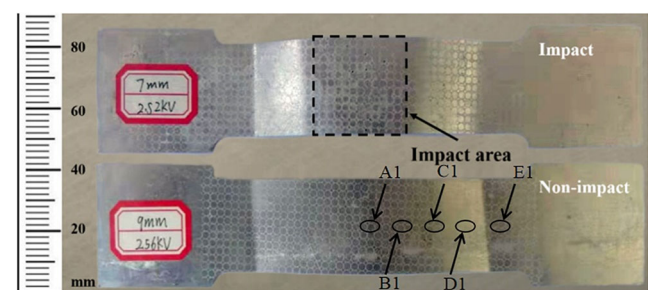
Table 3 The parameters of Cowper-Symonds model [19]

k	n	C	P
345MPa	0.148	7000s ⁻¹	0.96

The AA5754 aluminum alloy sheet with the thickness of 1 mm was used in the experiments. The shape and geometry of specimen are shown in Fig. 2. The length and width of the deformation area were 100 mm and 30 mm, respectively. There were rectangular clamping areas of 40 mm × 40 mm at both ends, and the specimen could be pre-deformed by the uniaxial tensile testing machine. The central area and the clamping area were transitioned by arc with radius of 5 mm. Before the experiment, the samples were cleaned with ethanol, and then the circular grids with diameter of 2.5 mm were printed on the surface by electrochemical etching for the deformation measurement. The grid strain measurement software of GMASystem was used to obtain the deformation of aluminum alloy sheet. The relative error of deformation measurement was less than 1.5%. With the same discharge voltage of 2.5 kV, the impact between the specimen and die occurred when the impact distance d was 7 mm, but the impact did not appear when the impact distance d was equal to or larger than 9 mm. For the hybrid quasi-static and dynamic forming experiments, the aluminum alloy sheet was pre-deformed with the quasi-static tensile strain of 5%.

2.2 Numerical model

The numerical simulation of coupled electromagnetic and structure fields was used to investigate the EMF processes. The sheet, coil, groove, and die were modeled by finite element method (FEM), as shown in Fig. 3, and the surrounding air field was considered by boundary element method (BEM). Considering the electromagnetic field simulation in the sheet, the sheet was meshed with hexahedral solid elements, and the thickness direction is divided into three layers. The sheet, coil, and groove were meshed with hexahedral solid elements, and the die was discretized with shell elements. The grooves, coils, and dies were defined as rigid bodies. The time increments of electromagnetic field and structure field were both 1 μs, and

**Fig. 4** The specimens after die forming and free forming

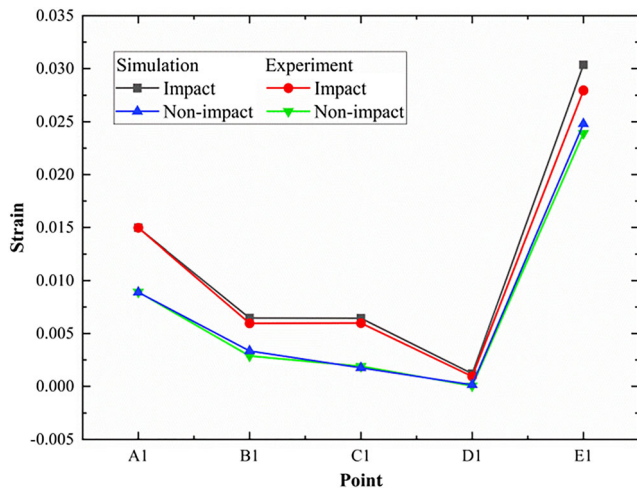


Fig. 5 Comparison of simulated and experimental strains after die forming and free forming

the total time of simulation was 200μs. The electromagnetic parameters are listed in Table 1.

The density of AA5754 aluminum alloy sheet is 2780 kg m⁻³. The Young’s modulus and Poisson’s ratio are 70 GPa and 0.33. In order to predict the damage evolution, the GTN model [18] was used to represent the plastic behavior of AA5754 aluminum alloy sheet as follows,

$$\phi = \frac{\sigma_M^2}{\sigma^2} + 2q_1f^* \cosh\left(\frac{3q_2\sigma_H}{2\sigma}\right) - 1 - (q_1f^*)^2 = 0 \quad (1)$$

where σ_M is the von Mises equivalent stress, σ is the yield stress, σ_H is the mean hydrostatic stress, q_1 and q_2 are the material parameters, and f^* is the effective void volume fraction. The voids only nucleate when stretched. The parameters of GTN model are shown in Table 2. The strain-rate-dependent hardening behavior of aluminum alloy sheet was characterized by the Cowper-Symonds model as follows,

$$\bar{\sigma} = (k\bar{\epsilon}^n) \left[\left(1 + \left(\frac{\dot{\epsilon}}{C} \right)^P \right) \right] \quad (2)$$

where ϵ_P is the equivalent plastic strain, $\dot{\epsilon}$ is the strain rate, k is the strength coefficient, n is the hardening exponent, and C and P are strain-rate hardening parameters. The parameters of Cowper-Symonds model are presented in Table 3.

3 Results and discussions

3.1 Free forming and die forming of aluminum alloy sheet without pre-deformation

After the electromagnetic free forming and electromagnetic die forming of AA5754 aluminum alloy sheet without pre-deformation, the non-impacted specimen and the impacted one are compared in Fig. 4. When the distance between the sheet and the die is 7 mm, the central area of specimen impacted the die. The experimental strains at five points of A1, B1, C1, D1, and E1 were measured by the circular grids, and compared with the simulated ones along the longitude direction, as shown in Fig. 5. The simulated results showed good agreement with the experimental ones for both the non-impacted and impacted specimens.

The curves of simulated stress triaxiality and void volume fraction at the central points of the impacted and non-impacted specimens are compared in Fig. 6. As shown in Fig. 6a, it was seen that the stress triaxiality became from negative to positive during the forming processes, because the specimens were subjected to the transient Lorentz forces along the thickness direction and then deformed under the tensile state along the longitude direction. However, the stress

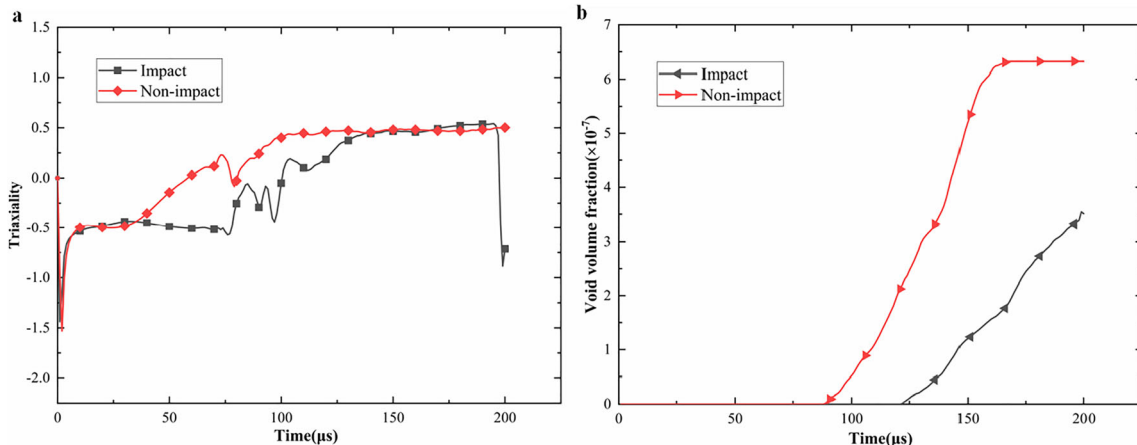
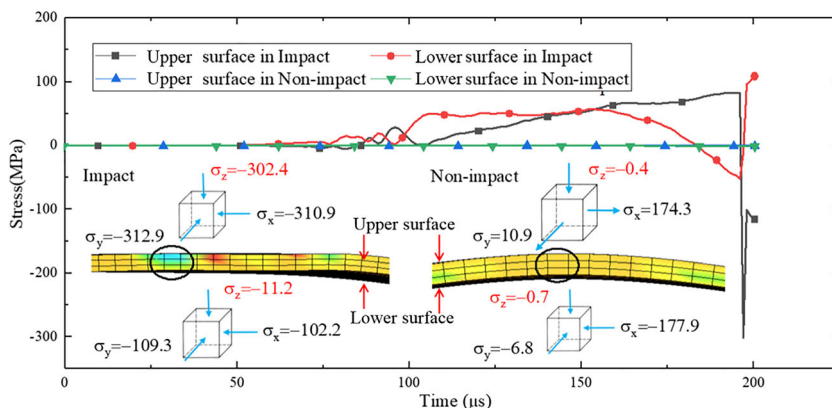


Fig. 6 Curves of stress triaxiality and void volume fraction during die forming and free forming. a Stress triaxiality. b Void volume fraction

Fig. 7 Simulated stress states on the upper and lower surfaces of non-impacted and impacted specimens



triaxiality was again changed to be negative at the time of 197 μs during the die forming while it remained to be positive during the free forming. Because the specimens were mainly deformed under the tensile state, the void volume fraction increased, as shown in Fig. 6b. However, due to the low deformation level at the central point of specimens, the void volume fractions were very small.

The simulated stresses at the central points of the non-impacted and impacted specimens are inspected in Fig. 7. By comparing the normal stress curves of the upper and lower surfaces were compared, it was found that the normal stress on the upper surface of impacted specimen suddenly decreased to be negative at 197 μs when the upper surface directly impacted the die. Meanwhile, the normal stresses of the non-impacted specimen were kept near zero. At 197 μs, the stress states at the central points of the non-impacted and impacted specimens were analyzed. For the non-impacted specimen, the tensile and compressive stresses were found on the upper and lower surface, respectively. The normal and transverse stresses on the upper and lower surfaces were very small. For the impacted specimen, the significant 3D compressive stresses were

found on the upper surface because of the die counter-impact, and the value of normal compressive stress reached up to 302.4 MPa. Due to the stress wave propagation, the modest compressive stresses were found on the lower surface of specimen.

The simulated stresses along the symmetric axis on the lower and upper surfaces of the impacted and non-impacted specimens are presented in Fig. 8. The stresses on the upper surface were positive, and the ones on the lower surface were close to zero. It was assumed that the lower surfaces were subjected to the quasi-uniform Lorentz forces, and the upper surfaces endured the large deformations under the tensile state.

3.2 Free forming and die forming of aluminum alloy sheet with pre-deformation

In order to study the effects of die counter-impact on aluminum alloy sheet during the hybrid quasi-static and dynamic process or EMAS, the specimens were previously deformed with the quasi-static tensile testing machine to reach the pre-deformation of 5% and then the free forming and die forming

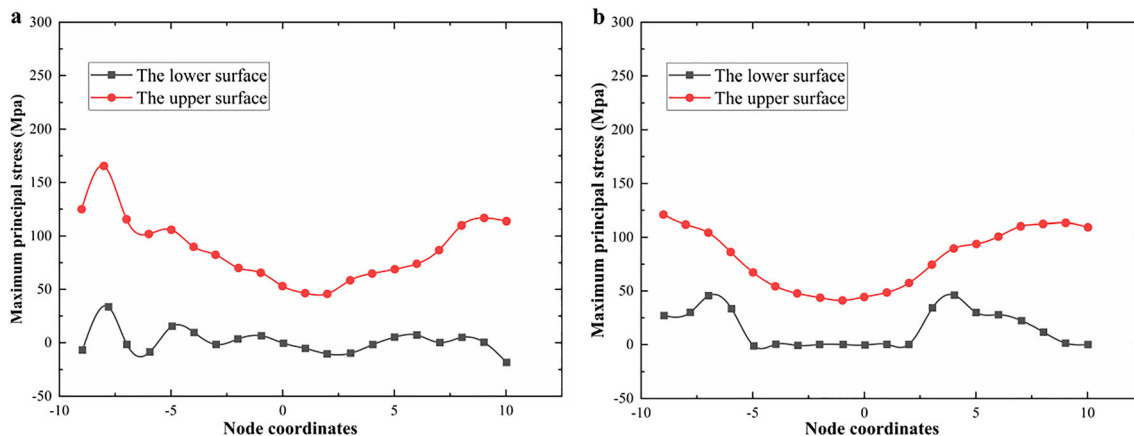


Fig. 8 Simulated stress along the symmetric axis of the specimens. **a** Die forming. **b** Free forming

experiments were carried out with the pre-deformed specimens, as shown in Fig. 9. The experimental and simulated strains at five points of A2, B2, C2, D2, and E2 were compared in Fig. 10. The discrepancies between the simulated and experimental results were small for the non-impacted and impacted specimens.

The curves of simulated stress triaxiality and void volume fraction at the central points of the impacted and non-impacted specimens with pre-deformation are presented in Fig. 11. While the stress triaxiality of the impacted specimen became negative due to the die counter-impact at the end of simulation, the stress triaxiality of the non-impacted specimen was unchanged, as shown in Fig. 11a. The void volume fraction of specimens after deformation was about 1.56%, and it increased with the sequential deformation. However, the void volume fraction of the impacted specimen suddenly decreased when the stress triaxiality became negative, as shown in Fig. 11b. Compared with the change of void volume fraction in Fig. 6b, it was seen that the void volume fraction of the pre-deformed specimen was reduced much more significantly.

The simulated stresses at the central points of the non-impacted and impacted specimens with pre-deformation are shown in Fig. 12. It was seen that the normal stresses on the upper and lower surfaces of the impacted specimen reached up to -358.7 MPa and -64.7 MPa, while those of the non-impacted specimen were always close to zero. The unignorable normal stresses were generated by the die counter-impact; the stress triaxiality and the void volume fraction were reduced.

The simulated stresses along the symmetric axis on the lower and upper surfaces of the impacted and non-impacted specimens with pre-deformation are compared in Fig. 13. The stresses at the impacted zone of the upper surface were obviously lower due to the die counter-impact, while the stresses on the upper surface of the non-impacted specimen were high. The stresses on the lower surface of the impacted and non-impacted specimens were very close to zero. Compared with the stress changes of specimens without pre-deformation in Fig. 8, the tensile stresses on the impacted surface of the pre-deformed specimen were reduced more significantly.

3.3 Comparisons of microstructure and hardness

The optical microscope was used to investigate the voids of specimens after free forming without pre-deformation, die forming without pre-deformation, free forming with pre-deformation, and die forming with

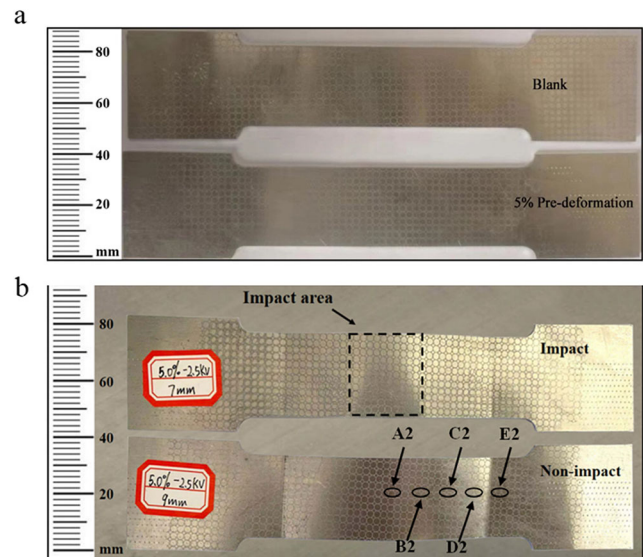


Fig. 9 The specimens of hybrid quasi-static and dynamic forming. **a** The pre-deformed specimen. **b** The specimens after die forming and free forming with pre-deformation

pre-deformation, as shown in Fig. 14. It was seen that the number and size of voids were smaller for the specimens without pre-deformation, and the number and size of voids were the largest for the specimen with pre-deformation. This might be because of pre-deformation and stretching, the initial damage of the workpiece was accumulated, and the initial void volume fraction was larger. Furthermore, the number and size of voids became much smaller for the specimen after die forming with pre-deformation than those for the specimen after free forming with pre-deformation. This phenomenon

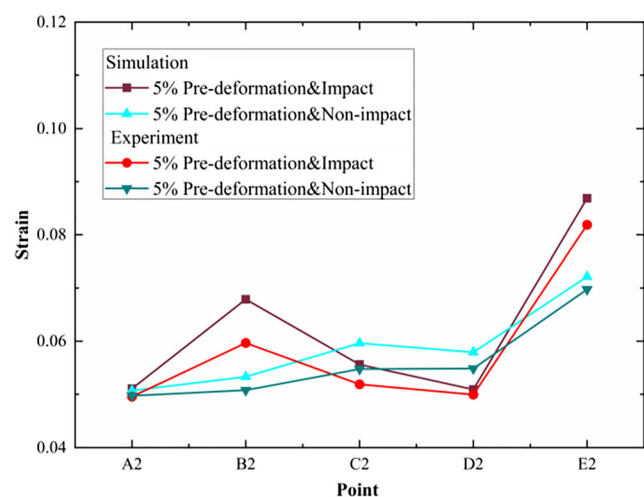


Fig. 10 Comparison of simulated and experimental strains after hybrid quasi-static and dynamic forming

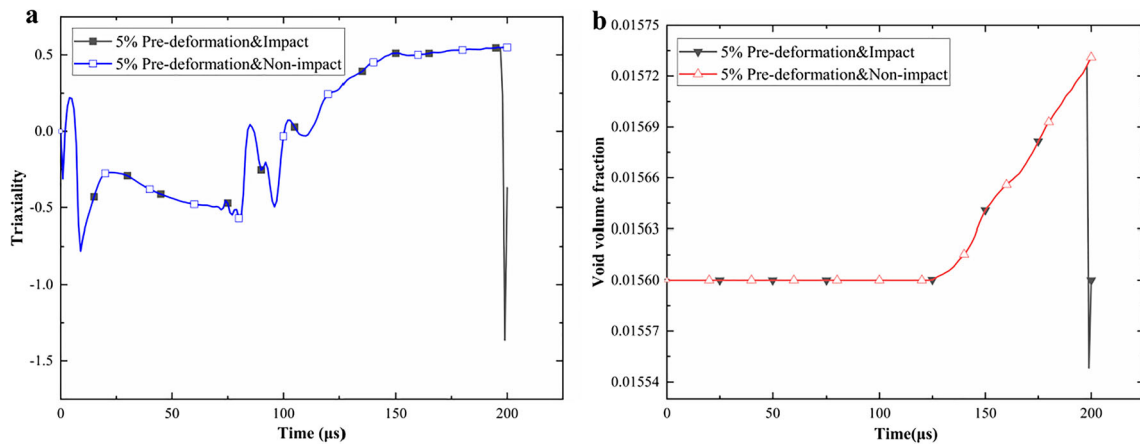
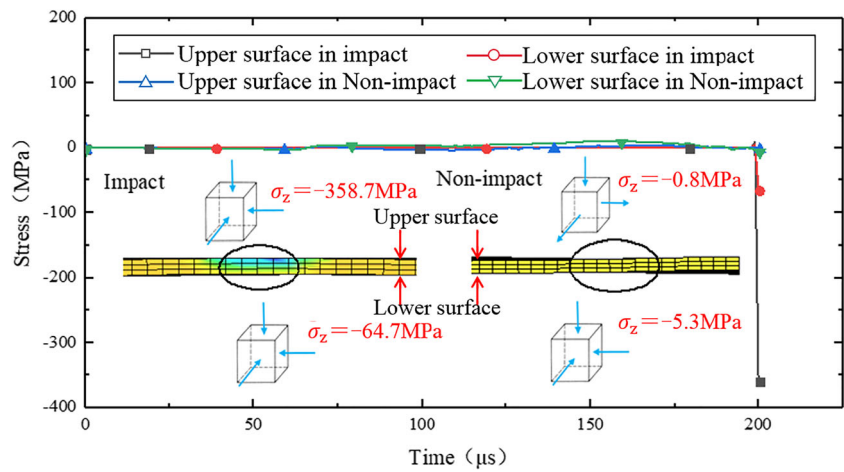


Fig. 11 Changes of stress triaxiality and void volume fraction of sheet metal after die forming and free forming in electromagnetic hybrid forming. **a** Stress triaxiality. **b** Void volume fraction

Fig. 12 Simulated stress states on the upper and lower surfaces of non-impacted and impacted specimens with pre-deformation



verified that the impact effect in the electromagnetic hybrid forming could play a good role in inhibiting the damage of the workpiece.

The Vickers hardness of the specimens after free forming without pre-deformation, die forming without pre-deformation, free forming with pre-deformation,

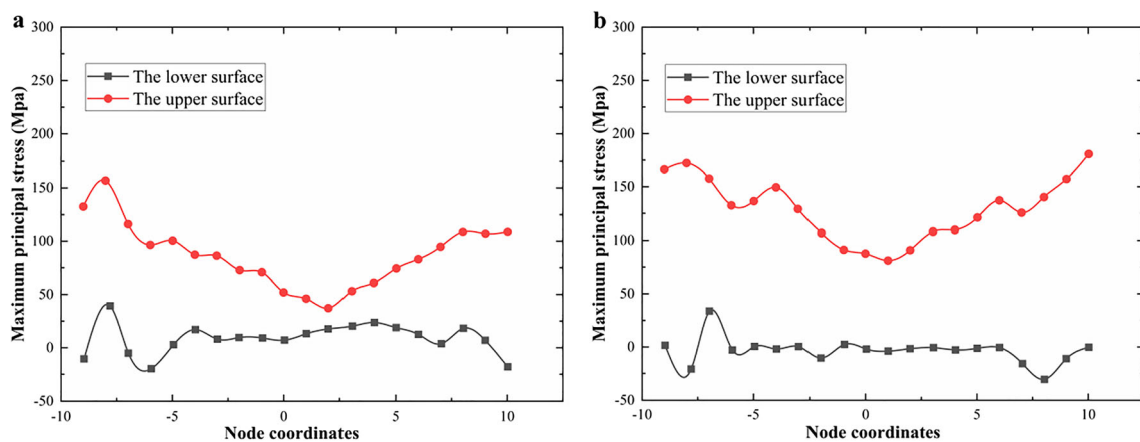
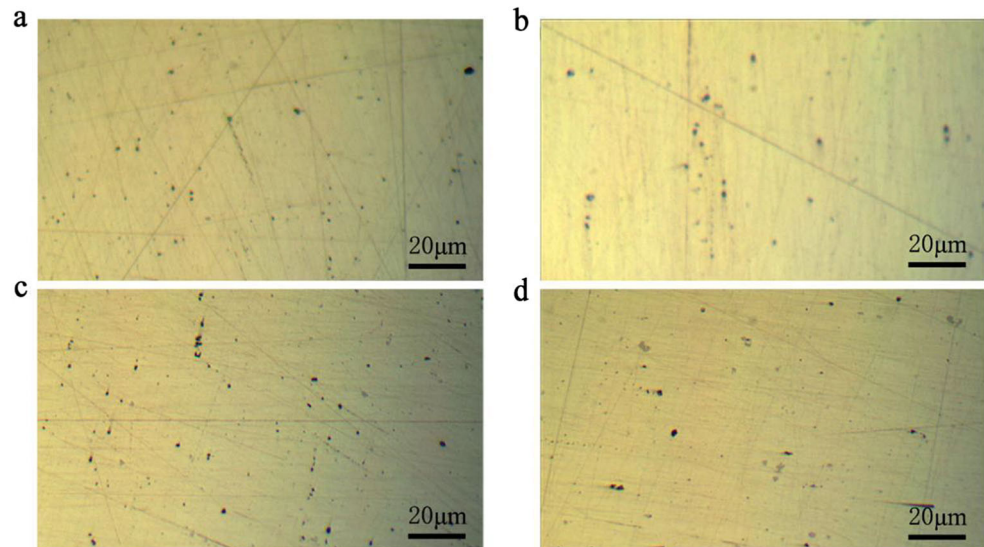


Fig. 13 Simulated stress along the symmetric axis of the specimens with pre-deformation. **a** Die forming. **b** Free forming

Fig. 14 Metallographic map of specimen. **a** Free forming without pre-deformation. **b** Die forming without pre-deformation. **c** Free forming with pre-deformation. **d** Die forming with pre-deformation



and die forming with pre-deformation is compared in Fig. 15. By comparing the hardness of the non-impacted and impacted specimens, it was seen that the hardness of aluminum alloy sheet was enhanced by the die counter-impact. By comparing the hardness of the specimens without and with pre-deformation, it was seen that the work hardening caused by plastic deformation enhanced the hardness of the aluminum alloy plate. Therefore, the hardness of the specimen after die forming with pre-deformation was the highest. This phenomenon verified that the impact effect in the electromagnetic hybrid forming could increase the surface hardness of the sheet metal, thereby improving the quality of the formed parts, which had an extremely positive effect on the production of high-quality products.

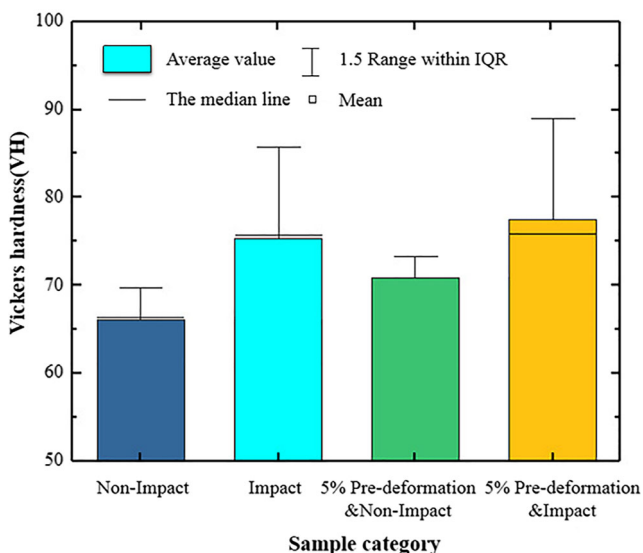


Fig. 15 Comparison of Vickers hardness

4 Conclusions

The effects of die counter-impact on aluminum alloy sheet during different EMF processes were investigated by simulation and experiment. The results showed the great potentials of the hybrid quasi-static and dynamic forming processes with die counter-impact for setting product properties beyond shaping. The main conclusions are as follows:

1. For the electromagnetic free forming and electromagnetic die forming of aluminum alloy sheet without pre-deformation, the impact effect of die forming could reduce the void volume fraction and improve the potential damage of the sheet. In this process, the impact action changed the stress distribution level of the sheet metal, which led to an increase in the stress difference between the upper and lower surfaces. At the same time, the impact area presented a three-way compression stress state, which made the size of the voids smaller from the squeezing action. The number of voids was reduced, which led to a decrease in the void volume fraction.
2. In the hybrid quasi-static and dynamic forming processes, the initial damage of the sheet metal after the sheet metal pretreatment was increased. Under the observation of the optical microscope, the number and size of voids were increased significantly. After electromagnetic bulging, the number of voids in die forming was less than that in free forming, and the damage reduction was more obvious, even lower than the initial void volume fraction, and the damage improvement effect was more obvious. At the same time, the impact action changed the stress state of the upper and lower surfaces of the sample, making the residual stress distribution more uniform. The hardness of the impact surface was strengthened, and the forming quality of the sample was improved.

Author contribution Zhenghua Meng and Shangyu Huang conceived and designed the work. Yangzhe Lin and Xiaoyong Zeng carried out the experiments and provided figures and tables. Yangzhe Lin and Wei Liu analyzed the data and edited the manuscript. Wei Liu reviewed and improved the manuscript.

Funding This work was supported by the National Natural Science Foundation of China (Grant No. 52005374) and Natural Science Foundation of Hubei Province (Grant No. 2019CFB196).

Data availability The datasets used or analyzed during the current work are available from the corresponding author on reasonable request.

Declarations

Ethics approval This work complies with the ethical standards set out by Springer.

Consent to participate Not applicable.

Consent to publish Not applicable.

Competing interests The authors declare no competing interests.

References

- Li J, Li L, Wan M, Yu H, Liu L (2018) Innovation applications of electromagnetic forming and its fundamental problems. *Procedia Manuf* 15:14–30
- Tekkaya AE, Allwood JM, Bariani PF, Bruschi S, Cao J, Gramlich S, Groche P, Hirt G, Ishikawa T, Löbbecke C, Lueg-Althoff J, Merklein M, Misiolek WZ, Pietrzyk M, Shivpuri R, Yanagimoto J (2015) Metal forming beyond shaping: predicting and setting product properties. *CIRP Ann Manuf Technol* 64:629–653
- Tekkaya AE, Khalifa NB, Hering O, Meya R, Myslicki S, Walther F (2017) Forming-induced damage and its effects on product properties. *CIRP Ann* 66(1):281–284
- Psyk V, Risch D, Kinsey BL, Tekkaya AE, Kleiner M (2011) Electromagnetic forming—a review. *J Mater Process Technol* 211(5):787–829
- Cui X, Li J, Mo J, Fang J, Zhou B, Xiao X, Feng F (2016) Incremental electromagnetic-assisted stamping (IEMAS) with radial magnetic pressure: a novel deep drawing method for forming aluminum alloy sheets. *J Mater Process Technol* 233:79–88
- Vohnout VJ (1998) A hybrid quasi-static/dynamic process for forming large sheet metal parts from aluminum alloys. The Ohio State University
- Shang J, Daehn G (2011) Electromagnetically assisted sheet metal stamping. *J Mater Process Technol* 211(5):868–874
- Imbert JM, Winkler SL, Worswick MJ, Oliveira DA, Golovashchenko S (2005) The effect of tool-sheet interaction on damage evolution in electromagnetic forming of aluminum alloy sheet. *J Eng Mater Technol* 127(1):145–153
- Golovashchenko SF (2007) Material formability and coil design in electromagnetic forming. *J Mater Eng Perform* 16(3):314–320
- Iriondo E, Gutiérrez MA, González B, Alcaraz JL, Daehn GS (2011) Electromagnetic impulse calibration of high strength sheet metal structures. *J Mater Process Technol* 211(5):909–915
- Kim J, Noh HG, Song WJ, Kang BS (2014) Comparative numerical analysis of sheet formed into a V-shaped die using conventional and electromagnetic forming processes. *Adv Mech Eng* 6:240789
- Su H, Huang L, Li J, Ma F, Huang P, Feng F (2018) Two-step electromagnetic forming: a new forming approach to local features of large-size sheet metal parts. *Int J Mach Tools Manuf* 124:99–116
- Liu W, Zou X, Huang S, Lei Y (2019) Electromagnetic-assisted calibration for surface part of aluminum alloy with a dedicated uniform pressure coil. *Int J Adv Manuf Technol* 100(1–4):721–727
- Feng F, Li J, Zhang Y, Huang L, Su H, Cao S, Shao G, Chen R (2020) Microstructure evolution of 5052 aluminum sheet in electromagnetic high-speed impact. *Metals* 10(5):564
- Zeng X, Meng Z, Liu W, Huang S, Zhou S, Lin Y (2020) Deformation behaviour and damage evolution of aluminium alloy sheet in electromagnetic forming with uniform pressure actuator. *Int J Adv Manuf Technol* 109(3):745–754
- Feng F, Li J, Huang L, Su H, Li H, Zhang Y, Cao S (2021) Formability enhancement of 5052 aluminium alloy sheet in electromagnetic impaction forming. *Int J Adv Manuf Technol* 112(9):2639–2655
- Kamal M, Daehn GS (2007) A uniform pressure electromagnetic actuator for forming flat sheets
- Needleman A, Tvergaard V (1984) An analysis of ductile rupture in notched bars. *J Mech Phys Solids* 32(6):461–490
- Noh HG, Lee K, Kang BS, Kim J (2016) Inverse parameter estimation of the Cowper-Symonds material model for electromagnetic free bulge forming. *Int J Precis Eng Manuf* 17(11):1483–1492

Publisher's note Springer Nature remains neutral with regard to jurisdictional claims in published maps and institutional affiliations.